BIOLOGICAL CRYSTALLOGRAPHY

ISSN 1399-0047

Intercalating dyes for enhanced contrast in second-harmonic generation imaging of protein crystals

Justin A. Newman,‡ Nicole M. Scarborough,‡ Nicholas R. Pogranichniy, Rashmi K. Shrestha, Richard G. Closser, Chittaranjan Das and Garth J. Simpson*

Department of Chemistry, Purdue University, 560 Oval Drive, West Lafayette, IN 47906, USA. *Correspondence e-mail: gsimpson@purdue.edu

Received 27 March 2015
Accepted 27 April 2015

Edited by R. J. Read, University of Cambridge, England

‡ These authors contributed equally to this work.

Keywords: SHG; protein crystals; high-throughput screening; dye.

Supporting information: this article has supporting information at journals.iucr.org/d

The second-harmonic generation (SHG) activity of protein crystals was found to be enhanced by up to ∼1000-fold by the intercalation of SHG phores within the crystal lattice. Unlike the intercalation of fluorophores, the SHG phores produced no significant background SHG from solvated dye or from dye intercalated into amorphous aggregates. The polarization-dependent SHG is consistent with the chromophores adopting the symmetry of the crystal lattice. In addition, the degree of enhancement for different symmetries of dyes is consistent with theoretical predictions based on the molecular nonlinear optical response. Kinetics studies indicate that intercalation arises over a timeframe of several minutes in lysozyme, with detectable enhancements within seconds. These results provide a potential means to increase the overall diversity of protein crystals and crystal sizes amenable to characterization by SHG microscopy.

1. Introduction

Recently, owing to the growing number of new protein targets for crystallization [an annual growth of ∼11% for protein crystal structures entered into the Protein Data Bank (PDB); Abad-Zapatero, 2012], the need for high-throughput technologies for protein crystal analysis has emerged. Currently, numerous imaging modalities are employed for scoring protein crystal 'hits' during the crystallization-condition screening process. Several instances of fluorescence imaging techniques such as two-photon excited UV fluorescence (TPE-UVF; Madden *et al.*, 2011), UV fluorescence (UVF; Vernede *et al.*, 2006; Judge *et al.*, 2005), covalent modification of the protein with a fluorophore (Forsythe *et al.*, 2006) and noncovalent fluorescent molecule intercalation (Groves *et al.*, 2007) have appeared in the recent literature. TPE-UVF and UVF utilize the intrinsic fluorescent properties of aromatic residues, for example tryptophan, found in most proteins to provide contrast (Madden *et al.*, 2011). However, UVF and TPE-UVF are limited to proteins with high intrinsic fluorescence. For proteins that do not exhibit strong intrinsic fluorescence (owing to a lack of tryptophan), such as insulin, UVF has been used for imaging (Vernede *et al.*, 2006). However, exposing protein crystals to a UV-C band excitation laser has been shown to damage disulfide bonds within the protein (Wien *et al.*, 2005). By covalently modifying proteins with fluorophores, researchers have been able to circumvent the need for intrinsic fluorescence and damaging laser wavelengths to visualize proteins (Forsythe *et al.*, 2006). However, this method adds a further sample-handling step, and studies have shown that covalent modification can adversely influence

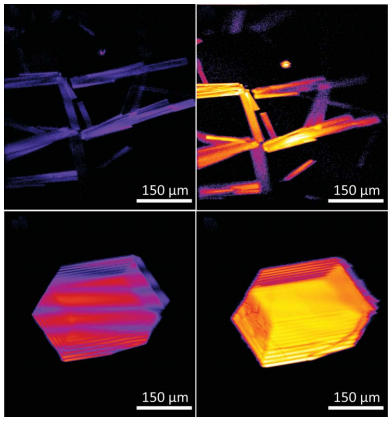

the folding structure of the protein (Groves *et al.*, 2007). All of the abovementioned techniques suffer from a major limitation owing to a lack of selectivity for crystalline protein, producing nonzero signals from crystalline proteins, amorphous protein aggregates and proteins in solution.

Second-harmonic generation (SHG) microscopy has been shown to be a complementary technique for selective imaging of protein crystals (Kissick *et al.*, 2009). SHG, or the frequency doubling of light, can arise when noncentrosymmetric crystalline material is illuminated by sufficiently intense light, with negligible contributions from disordered media such as protein aggregates. Recently, SHG microscopy has been successfully developed for the automated analysis of 96-well plates (Kissick *et al.*, 2011), assessing crystal quality through polarization analysis (DeWalt *et al.*, 2013) and the rapid centering of crystals on a synchrotron beamline (Kissick *et al.*, 2013; Madden *et al.*, 2013). However, current SHG microscopy techniques can only detect an estimated 84% of known protein crystal structures, with crystals exhibiting SHG activities spanning several orders of magnitude (Haupert *et al.*, 2012). For smaller crystals or for high-throughput screening applications with shorter signal integration times, this coverage value will be correspondingly reduced, suggesting the need for improvements in the signal-to-noise ratio (SNR) for crystal detection. The SHG response varies considerably depending upon the protein, the protein orientation within the lattice and the symmetry of the lattice, the latter of which is the main driving force behind the inability to detect ∼16% of the current PDB entries. A detailed discussion of the relationships between symmetry, structure and SHG activity of the different protein crystal space groups can be found in Haupert *et al.* (2012). In brief, crystal classes with 422 (D_4) and 622 (D_6) symmetry are relatively weak for SHG, with coherent SHG strictly forbidden only in the 432 (O) symmetry class. Improving the detection limits of SHG could increase the coverage of protein crystals amenable to SHG detection, reduce the timeframe required for protein crystal imaging by SHG and allow the detection of increasingly smaller crystals at the early stages of crystallization. Improving any one of these aspects may significantly reduce the amount of time that it takes to solve a structure of a novel protein.

In an effort to decrease the number of false negatives for crystallization-condition screening and increase the SNR for protein crystal detection, we demonstrate the use of SHG-active dyes to enhance the SHG response of protein crystals. By incorporating dyes, either prior to or post crystallization, the dyes adopt a symmetry mirroring that of the underlying protein lattice to produce enhanced coherent SHG. The enhanced SHG activity can then reduce the false-negative rate for SHG microscopy by allowing the detection of weakly SHG active crystals and small crystallites that would otherwise go unnoticed. The detection of exceedingly smaller crystals has aided recent advances in X-ray free-electron diffraction (Liu *et al.*, 2013). Using a 'diffract-and-destroy' approach, in which hundreds of crystals are exposed once, the data from all of the individual diffraction events can be pooled to solve a structure.

Reducing false negatives by the intercalation of SHG-active dyes can potentially lead to a larger pool of potential crystal leads, increasing the chances of finding a condition that yields high diffraction-quality crystals. Once potential crystallization-condition candidates have been determined, the dyes can be omitted while the conditions are optimized to yield high-quality crystals, similar to the approaches already established using trace labelling with fluorescent dyes (Forsythe *et al.*, 2006). The present study is designed to characterize the symmetry properties and enhancements of representative SHG phores within selected protein crystal lattices.

2. Experimental methods

The crystallization of lysozyme was adapted from a previous method by Yaoi *et al.* (2004) and is briefly described here. Chicken egg-white lysozyme was purchased from Sigma–Aldrich (catalog No. L6876). A 25.0 mg ml^{-1} lysozyme solution was prepared in 0.5 ml nanopure water and filtered through a 0.2 µm pore-size filter. Crystallization was achieved with a 7%(*w*/*w*) NaCl solution in acetate buffer prepared by mixing 3.75 ml of a 1:10 dilution of glacial acetic acid, 0.295 g sodium acetate and 40 g NaCl and diluted to 500 ml with nanopure water. Tetragonal lysozyme crystals of space group $P4_32_12$ were grown in 96-well crystallization plates (Corning). 100 µl of the NaCl–acetate buffer solution was added to the reservoir well. 1 µl of NaCl–acetate buffer solution and 1 µl of lysozyme solution were added to the crystallization wells. The wells were sealed with tape and allowed to crystallize overnight.

The crystallization of $I222$ and $P2_12_12_1$ polymorphs of glucose isomerase has been described elsewhere (DeWalt *et al.*, 2014) and is only briefly described here. A crystalline suspension of glucose isomerase (Hampton Research) was dialyzed against 10 mM HEPES, 1 mM $MgCl_2$ and 100 mM HEPES, 10 mM $MgCl_2$. To obtain the $P2_12_12_1$ polymorph the glucose isomerase solution was concentrated to 35 mg ml^{-1} and was crystallized in 2.0 M ammonium sulfate pH 7.4. The $I222$ polymorph was obtained by concentrating to 26 mg ml^{-1} and was crystallized in 0.7 M sodium citrate tribasic dehydrate pH 7.

Crystals of the catalytic domain of the JAMM family metallo-deubiquitinating enzyme (DUB) from *Schizosaccharomyces pombe* (Sst2^{cat}) were obtained using a method previously described elsewhere (Shrestha *et al.*, 2014). The domain was expressed in *Escherichia coli* as a recombinant protein fused to a glutathione *S*-transferase (GST) tag at the N-terminus. The protein was purified using glutathione agarose beads and the GST tag was cleaved with PreScission protease (GE Biosciences). For crystallization, Sst2^{cat} was concentrated to 20 mg ml^{-1} in a buffer consisting of 50 mM Tris–HCl, 50 mM NaCl, 1 mM DTT pH 7.6. Crystallization was performed by sitting-drop vapor diffusion at room temperature. Crystals of Sst2^{cat} were grown from a reservoir consisting of 0.2 M ammonium phosphate dibasic pH 8.0, 20%(*w*/*v*) polyethylene glycol (PEG) 3350. The crystals were

obtained from a drop consisting of 1.5 µl protein solution and 1.5 µl reservoir solution.

Solutions of 500 µ*M* malachite green oxalate salt (Sigma–Aldrich) and *trans*-4-[4-(dimethylamino)styryl]-1-methylpyridinium iodide (Sigma–Aldrich) were prepared in ethyl acetate. The dye was introduced into the protein crystals by removing the tape and adding 1 µl of the dye solution to each small well. The ethyl acetate was allowed time to evaporate before the wells were resealed and left for 10 min to allow the dye to intercalate into the crystals.

SHG images were obtained using a custom-built beam-scanning SHG microscope. Beam scanning was performed with a resonant vibrating mirror (∼8 kHz; EOPC) along the fast-axis scan and a galvanometer (Cambridge) for slow-axis scanning. The incident beam was provided *via* an 80 MHz Ti:sapphire pulsed laser (Spectra-Physics Mai Tai) with 100 fs pulses at 800 nm. The beam was focused on the sample with a 10× objective with a working distance of 1.6 cm (Nikon; NA = 0.30). The incident wavelength was 1000 nm, with 90 mW average power at the sample. 2000 frames were collected and averaged with an average acquisition time of about 2 min. The SHG signal was collected with dichroic mirrors and narrow-bandpass filters centered about 500 nm placed before the photomultiplier tube detectors (PMTs). The incident beam was horizontally polarized and the vertical and horizontal components were collected separately. *MatLab* code was written in-house to control the scanning mirrors and communication with the data-acquisition electronics. *ImageJ* was used to analyze and produce SHG images.

Crystals of proteinase K (space group $P4_32_12$) were obtained by screening against the Crystal Screen HT kit (Hampton Research) by sitting-drop vapor diffusion in a three-drop 96-well plate (Corning). Two of the crystallization wells contained 1 µl 20 mg ml^{-1} proteinase K (Sigma) in 25 m*M* HEPES pH 7.0 with 1 µl of the respective crystal screen solution. The two wells contained dye concentrations of either 0 or 50 µ*M*. The crystallization was performed with both malachite green and crystal violet dyes. The well plates were imaged using the automated SHG microscope SONICC (Formulatrix).

3. Results and discussion

The results of malachite green intercalation into lysozyme protein crystals are summarized in Fig. 1. Native tetragonal lysozyme crystals generated weak SHG signals, as exemplified in Fig. 1(*a*), with significant signal averaging performed to visualize the protein crystals. The addition of an SHG-active dye was found to significantly increase the SHG activity and SNR of the image over a total intercalation time scale of 12 min (Figs. 1*b*, 1*c* and 1*d*). While the SHG enhancement is highly variable owing to the dependence on crystal orientation and the challenge in accurately quantifying the weak initial responses, an average enhancement of ∼4500-fold was achieved for the intercalation of malachite green into lysozyme protein crystals.

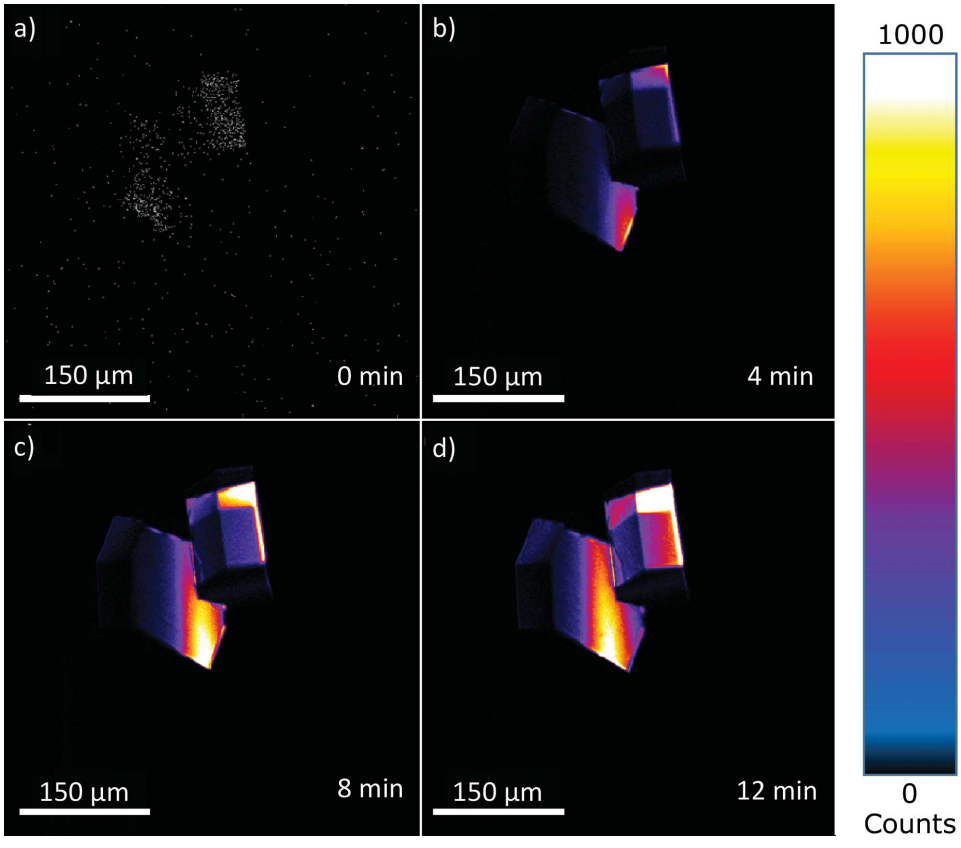

Figure 1
Intercalation of a 500 µ*M* solution of malachite green into lysozyme crystals. At time zero (*a*) there is no detectable SHG. The scale was adjusted to show low counts. Within minutes detectable signal was observed (*b*, *c*, *d*) with an overall SHG enhancement of ∼700 after 12 min of dye intercalation.

The universality of staining with an SHG phore was examined by intercalating malachite green and crystal violet into two different polymorphs of glucose isomerase. The results of the SHG enhancement for both the *I*222 and $P2_12_12_1$ polymorphs are shown in Fig. 2. Crystal violet was used to stain the *I*222 polymorph (Figs. 2*a* and 2*b*) owing to the use of citrate in the crystallization (see below). The enhancement of *I*222 glucose isomerase is only of the order of a threefold enhancement in SHG activity, which may be owing to differences in the degree of dye incorporation, the degree of dye ordering within the crystal or the lowered native nonlinear optical

Table 1
Proteinase K sparse-matrix screen.

Crystal screen hits from Crystal Screen HT with proteinase K with the addition of either no dye, 50 m*M* MG or 50 m*M* CV.

	No dye	CV	MG
Crystal hits	58†	23	62
Dye hits/no dye hits	—	23/58 (39.7%)	62/58 (106.9%)
Crystal hits with SHG	0 (0%)	16 (69.6%)	49 (79.0%)

activity of crystal violet relative to malachite green at the measurement wavelengths. The $P2_12_12_1$ polymorph was stained with malachite green and an enhancement of approximately one order of magnitude was observed (Figs. 2*c* and 2*d*).

Through experimentation with various different crystallization conditions, it was found that malachite green interacts with citrate and phosphate, resulting in a visible loss of the green color and likely reducing the resonance-enhanced SHG activity over time. For this reason, the structurally similar crystal violet was used for soaking crystals when citrate salts were used to induce crystallization. When added to the DUB crystals grown in ammonium phosphate and PEG, malachite green initially intercalated into the crystal and increased the inherent SHG intensity of the protein by ∼25-fold. However, within 10 min this signal began to decrease following an exponential decay, decreasing to about 10% of the original dye signal within 3 h (Fig. 3). This decrease in signal qualitatively tracked the visual loss of the green color within the wells. This effect can potentially be attributed to the PEG successfully competing with the protein for the dye, or a chelating effect from the phosphate, similar to the effect observed with citrate.

To further investigate the compatibility of the dyes with varying crystallization conditions, a set of 96-well sparse-matrix crystal screens was performed for the crystallization of proteinase K. Proteinase K was chosen as a model system because it crystallizes in a wide variety of different crystallization conditions. The breadth of conditions that could produce crystals for a single protein in a single space group allowed statistically significant assessments of the potential impact that dye incorporation may have on crystallizability. The results of the screen for malachite green (MG) and crystal violet (CV) are summarized in Table 1 and Supplementary Figs. S1 and S2. The 106.9% hit rate for crystallization in the presence of MG indicates that the presence of MG does not inhibit crystallization of the proteins, with the elevated hit rate well within the inherent variability for the crystallization of proteinase K without dye (found to be 28.9%). The crystal hit rate in the presence of MG, combined with no observable crystal morphology changes, is consistent with previous studies incorporating fluorescent dyes (Groves *et al.*, 2007; Padayatti *et al.*, 2012), which showed no significant effect on the crystallization, size, shape or diffraction quality of the protein crystals. The impact of CV on the crystallization behavior of the proteins and the absence of an impact for MG demonstrate the advantages of screening of a diversity of dyes to map 'dye space' for a given protein and set of conditions. Strong interactions between dyes and proteins at specific contact points within the lattice may potentially interfere with the crystallizability. However, the selection of a suite of SHG phores with substantial chemical and structural diversity can help to minimize the overall potential impact on crystallizability in high-throughput screening. It is worth

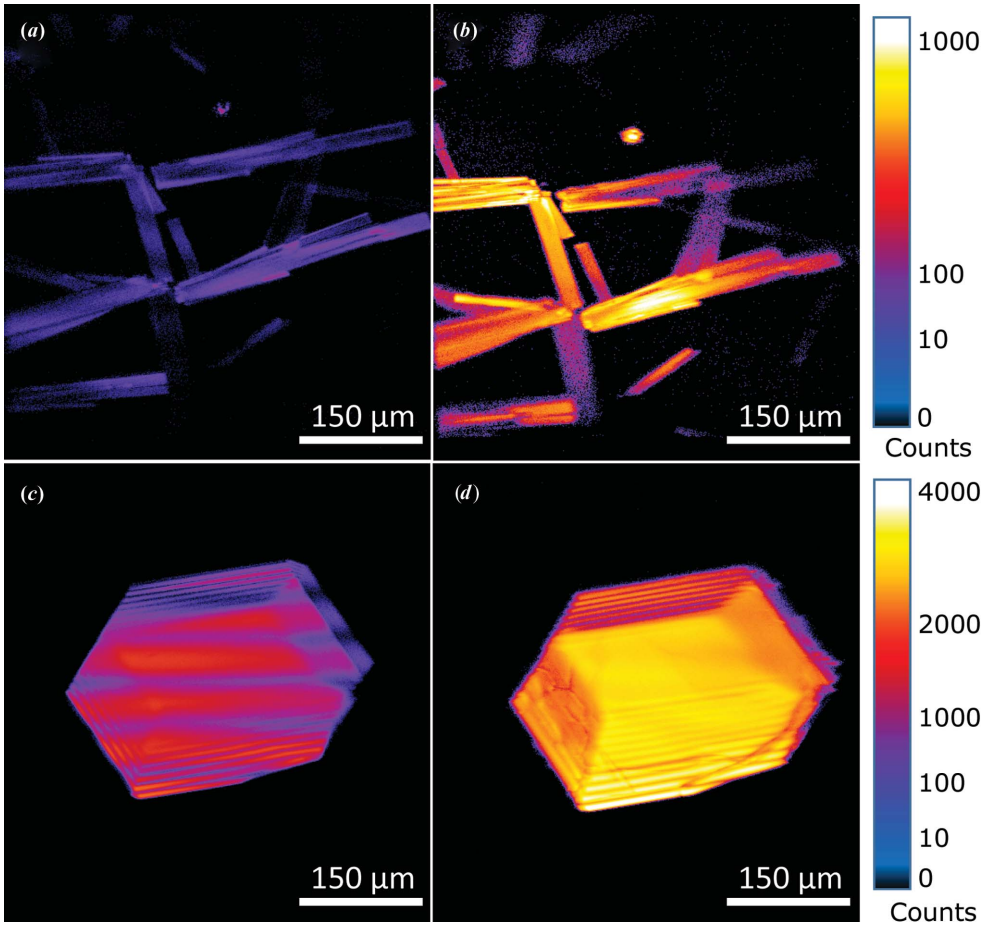

Figure 2
(*a*) Undyed $P2_12_12$ glucose isomerase crystals. (*b*) Intercalation of a 500 µ*M* solution of malachite green into the $P2_12_12$ crystals. (*c*) Undyed *I*222 glucose isomerase crystals. (*d*) Intercalation of a 500 µ*M* solution of crystal violet into the *I*222 crystals.

emphasizing that both CV and MG crystallization trials still resulted in numerous crystals that were clearly identifiable by SHG and amenable to automated detection, while similar unstained crystals were not.

Unlike fluorescence, coherent SHG is symmetry-forbidden from isotropic or disordered media. Therefore, the mechanism of image contrast and signal generation may not be trivially obvious. It is conjectured here that the presence of SHG arises from dye association at preferred locations within the protein (*e.g.* hydrophobic pockets), such that the dyes adopt the macromolecular symmetry of the lattice. Experiments were performed to test this hypothesis by measuring the polarization-dependent SHG and comparing the results with the expectations based on the lattice symmetry and the molecular symmetry.

The thermodynamically favored form of crystalline lysozyme is an aqueous environment is a tetragonal ($P4_32_12$) structure. The corresponding D_4 point group of the crystal lattice allows the following nonvanishing $\beta^{(2)}$ tensor elements in the crystal (Boyd, 2008; Shen, 1984),

$$\beta_{xyz} = -\beta_{yxz} = \beta_{xzy} = -\beta_{yzx}. \quad (1)$$

The local frame of the crystal is related to the laboratory frame through a rotation operation, expressed in terms of the Euler angles θ, ψ and φ, describing the tilt, twist and azimuthal rotation, respectively. In the laboratory frame for vertically polarized detection, the coparallel detected SHG $\chi^{(2)}$ tensor element is $\chi^{(2)}_{\rm VVV}$, while the cross-polarized tensor element is $\chi^{(2)}_{\rm VHH}$. For the four nonzero tensor elements in (1), the laboratory-frame response of a tetragonal lysozyme crystal oriented by a set of angles (θ, ψ, φ) relative to the vertical axis is given by the expression

$$\begin{aligned}\chi_{\rm VVV} &\propto -(\beta_{xyz}+\beta_{xzy}+\beta_{yxz}+\beta_{yzx})\sin^2\theta\cos\theta\sin\psi\cos\psi\\ \chi_{\rm VHH} &\propto (\beta_{xyz}+\beta_{xzy})\sin^2\theta\cos\psi\cos\varphi(\cos\psi\sin\varphi+\cos\theta\sin\psi\cos\varphi)\\ &+\ (\beta_{yxz}+\beta_{zyx})\sin^2\theta\sin\psi\cos\varphi(-\sin\psi\sin\varphi+\cos\theta\cos\psi\cos\varphi).\end{aligned} \quad (2)$$

If the equalities between the $\beta^{(2)}$ tensor elements in the tetragonal lysozyme lattice in (1) are applied, the coparallel and cross-polarized tensor elements simplify to the relations

$$\begin{aligned}\chi_{\rm VVV} &= 0,\\ \chi_{\rm VHH} &\propto \beta_{xyz}\sin^2\theta\sin\varphi\cos\varphi.\end{aligned} \quad (3)$$

Irrespective of the crystal orientation, the expression above demands that only cross-polarized SHG can be coherently produced by the tetragonal lysozyme lattice, consistent with previous experimental observations (Haupert *et al.*, 2012). All crystals of D_4 and D_6 symmetry share this same requirement. In contrast, the molecular tensor for malachite green has been found previously to be dominated by the β_{zxx} tensor element for SHG measurements with a fundamental wavelength of ~800 nm (Shi *et al.*, 1996), which can contribute to both coparallel and cross-polarized SHG depending on the molecular orientation. Experimentally, the SHG signal from native lysozyme crystals (without the SHG phore) was only detectable for cross-polarized SHG measured in transmission (Haupert *et al.*, 2012), consistent with the expectations based on symmetry. Therefore, the observation of a strong preference for cross-polarized SHG from lysozyme crystals incorporating the SHG phores would support a mechanism in which the dyes adopt the symmetry of the underlying crystal lattice.

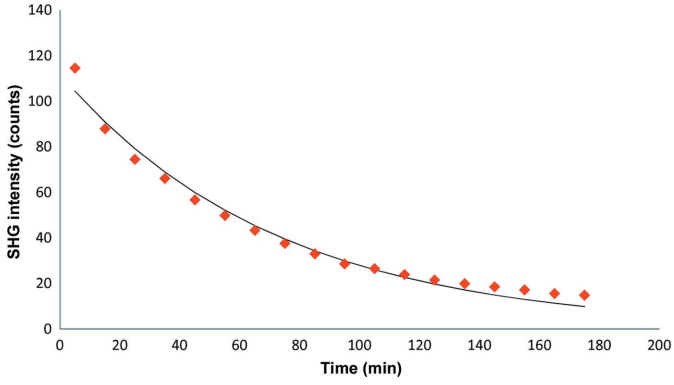

Figure 3
A 25-fold SHG enhancement was initially observed for the DUB crystal dyed with malachite green. The plot shows the resulting signal decay as a function of time for the SHG enhancement. Malachite green initially causes the expected increase in SHG intensity in the protein crystals, but the signal quickly decays as the phosphate salt interacts with the dye.

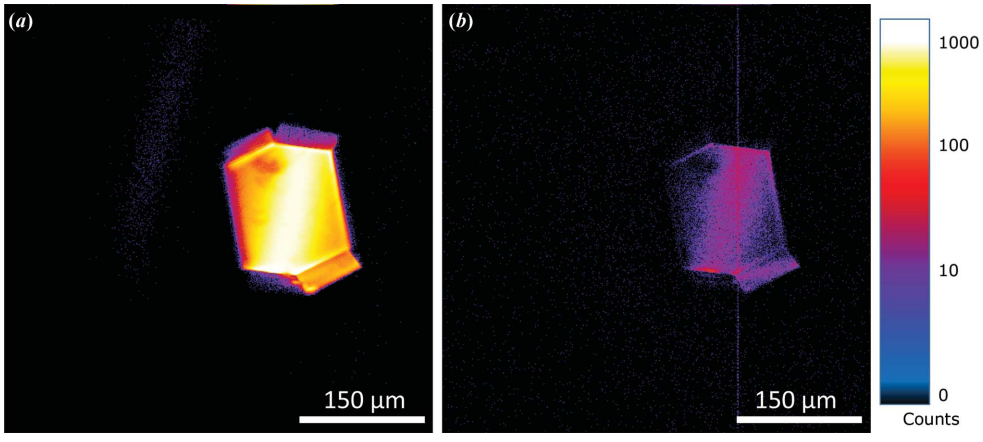

Figure 4
Cross-polarized (*a*) and coparallel (*b*) SHG images of lysozyme soaked in malachite green were acquired from the same crystal. The greater intensity found in the cross-polarized image supports the hypothesis that the dye is templated by the crystal lattice.

Polarization-dependent measurements of dye-incorporated lysozyme crystals are shown in Fig. 4. Consistent with the theoretical predictions for a templating interaction, the SHG intensity from the SHG-enhanced crystals is predominantly cross-polarized. This observation suggests that the SHG phore adopts the symmetry of the lattice, consistent with a preferred

and oriented association with the proteins in the lattice.

The diversity of enhancement factors upon dye soaking is noteworthy. In general, the greatest enhancements were observed for the protein crystals with the highest symmetry and the lowest native SHG activity (*e.g.* tetragonal lysozyme and proteinase K). Relatively modest enhancements of approximately an order of magnitude were observed in other cases (for example, MG with DUB and glucose isomerase). In previous work, a diversity of SHG activities spanning several orders of magnitude was predicted for native protein crystals. The large variability is attributed to protein orientation within the lattice in combination with the symmetry of the lattice (Haupert *et al.*, 2012). As a result, the observation here of enhancement factors spanning several decades is also not particularly surprising and is consistent with the general trends in SHG.

The preferentially greater enhancements observed with high-symmetry crystals is also consistent with theoretical predictions when using 'Λ-like' chromophores such as MG and CV. Dyes of this form still generally produce bright bulk-allowed SHG when arranged in lattices lacking polar order. Previous theoretical work suggests that the SHG activity will generally be optimized for chiral crystals containing chromophores, in which the low-lying transition moments are perpendicular to the charge-transfer axis (Wampler *et al.*, 2008; Ostroverkhov *et al.*, 2001). This molecular-design principle led to the consideration of MG and CV as potential candidates for crystal SHG phores. In contrast, the fraction of the total hyperpolarizability surviving the symmetry operations of the lattice is substantially reduced in 'rod-like' chromophores, in which the hyperpolarizability is dominated by interactions along a single internal axis within the chromophore (Wampler *et al.*, 2008). In this limit, the molecular tensor is dominated by the β_{zzz} tensor element. Because all three indices are interchangeable within the molecular tensor, this same interchangeability must also hold in the macroscopic $\beta^{(2)}$ tensor of the crystal. In the case of tetragonal lysozyme, this interchangeability requires all of the elements in (1) to also equal β_{zxy}, which is already zero from the symmetry operations of the lattice.

Experiments to test the prediction of stronger enhancements from Λ-like chromophores relative to rod-like chromophores were performed using the SHG-active dye *trans*-4-[4-(dimethylamino)styryl]-1-methylpyridinium iodide (DMI), in which the long molecular axis of the chromophore dominates the nonlinear optical activity. As shown in Fig. 5, the enhancement from the Λ-like malachite green was 4500-fold, while that from the rod-like DMI was only 30-fold. This value is an upper limit owing to DMI also producing a two-photon excited fluorescence background which may have interfered with the detection of the SHG.

4. Conclusion

The use of SHG-active dyes has been shown to enhance the SHG activity and increase the SNR for imaging protein crystals during the crystallization-condition screening process. Malachite green offered the strongest enhancements compared with crystal violet and DMI. However, crystal violet exhibited no significant interference from the presence of citrate salts, which were observed to reduce the resonance-enhanced SHG activity of malachite green. Polarization-dependent measurements were consistent with the SHG phores adopting the symmetry of the lattice, producing only cross-polarized SHG in studies of tetragonal lysozyme crystals. Enhancements ranging from 3 to >4000 were observed for three different proteins and multiple crystal polymorphs. The variability in the enhancement is likely to arise from a combination of multiple effects, including but not limited to differences in the initial SHG activity of the protein crystal, the degree of SHG-phore incorporation, the degree of ordering of the incorporated SHG phores and the inherent hyperpolarizability of the SHG phore.

Enhancement of the SHG activity of initial crystallization hits has the potential to offer several key practical advantages in high-throughput screening of crystallization conditions. Firstly, the nature of image contrast for SHG (*i.e.* no signal from aggregates or solubilized proteins but SHG from the crystalline state) is well suited for automated scoring, which can be a major bottleneck in high-density crystallization platforms (*e.g.* crystallization microchips or 1536-well plates). Dye-enhanced detection of promising crystallization conditions can be performed in low-volume crystallization platforms and then scaled up and optimized without the use of dyes for the production of high diffraction-quality crystals. By adopting the symmetry of the lattice, soaking with SHG

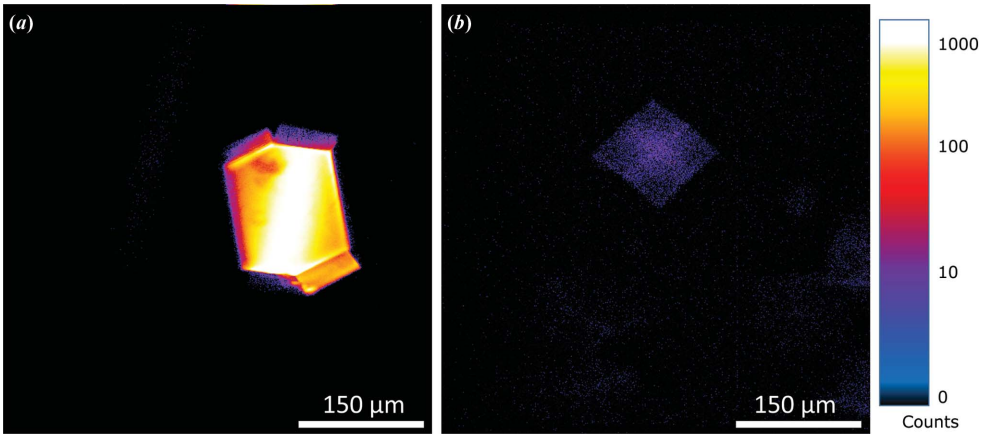

Figure 5
Signal enhancement from Λ-like chromophores *versus* rod-like chromophores. The intercalation of MG (*a*) shows an enhancement of ∼4500 fold. The addition of DMI (*b*) only achieved a 30-fold enhancement.

phores still provides the same selectivity for protein crystals afforded by SHG, with no coherent background produced from disordered proteins, including aggregates and proteins in solution, thereby reducing the number of false negatives for crystallization-condition screening by SHG microscopy.

Acknowledgements

The authors gratefully acknowledge support from NIH Grant No. R01GM-103910 from the NIGMS. JAN would also like to acknowledge the Purdue Research Foundation and the Henry B. Hass Fellowship for financial support. The authors are grateful to Emma DeWalt for invaluable help in preparing the samples for these experiments.

References

Abad-Zapatero, C. (2012). *Acta Cryst.* D**68**, 613–617.
Boyd, R. W. (2008). *Nonlinear Optics*, 3rd ed. Burlington, San Diego, London: Elsevier.
DeWalt, E. L., Begue, V. J., Ronau, J. A., Sullivan, S. Z., Das, C. & Simpson, G. J. (2013). *Acta Cryst.* D**69**, 74–81.
DeWalt, E. L., Sullivan, S. Z., Schmitt, P. D., Muir, R. D. & Simpson, G. J. (2014). *Anal. Chem.* **86**, 8448–8456.
Forsythe, E., Achari, A. & Pusey, M. L. (2006). *Acta Cryst.* D**62**, 339–346.
Groves, M. R., Müller, I. B., Kreplin, X. & Müller-Dieckmann, J. (2007). *Acta Cryst.* D**63**, 526–535.
Haupert, L. M., DeWalt, E. L. & Simpson, G. J. (2012). *Acta Cryst.* D**68**, 1513–1521.
Judge, R. A., Swift, K. & González, C. (2005). *Acta Cryst.* D**61**, 60–66.
Kissick, D. J., Dettmar, C. M., Becker, M., Mulichak, A. M., Cherezov, V., Ginell, S. L., Battaile, K. P., Keefe, L. J., Fischetti, R. F. & Simpson, G. J. (2013). *Acta Cryst.* D**69**, 843–851.
Kissick, D. J., Gualtieri, E. J., Simpson, G. J. & Cherezov, V. (2009). *Anal. Chem.* **82**, 491–497.
Kissick, D. J., Wanapun, D. & Simpson, G. J. (2011). *Annu. Rev. Anal. Chem.* **4**, 419–437.
Liu, W. *et al.* (2013). *Science*, **342**, 1521–1524.
Madden, J. T., DeWalt, E. L. & Simpson, G. J. (2011). *Acta Cryst.* D**67**, 839–846.
Madden, J. T. *et al.* (2013). *J. Synchrotron Rad.* **20**, 531–540.
Ostroverkhov, V., Petschek, R. G., Singer, K. D. & Twieg, R. J. (2001). *Chem. Phys. Lett.* **340**, 109–115.
Padayatti, P., Palczewska, G., Sun, W., Palczewski, K. & Salom, D. (2012). *Biochemistry*, **51**, 1625–1637.
Shen, Y. R. (1984). *The Principles of Nonlinear Optics*. New York: John Wiley & Sons.
Shi, X., Borguet, E., Tarnovsky, A. N. & Eisenthal, K. B. (1996). *Chem. Phys.* **205**, 167–178.
Shrestha, R. K., Ronau, J. A., Davies, C. W., Guenette, R. G., Strieter, E. R., Paul, L. N. & Das, C. (2014). *Biochemistry*, **53**, 3199–3217.
Vernede, X., Lavault, B., Ohana, J., Nurizzo, D., Joly, J., Jacquamet, L., Felisaz, F., Cipriani, F. & Bourgeois, D. (2006). *Acta Cryst.* D**62**, 253–261.
Wampler, R. D., Begue, N. J. & Simpson, G. J. (2008). *Cryst. Growth Des.* **8**, 2589–2594.
Wien, F., Miles, A. J., Lees, J. G., Vrønning Hoffmann, S. & Wallace, B. A. (2005). *J. Synchrotron Rad.* **12**, 517–523.
Yaoi, M., Adachi, H., Takano, K., Matsumura, H., Inoue, T., Mori, Y. & Sasaki, T. (2004). *Jpn. J. Appl. Phys.* **43**, L1318–L1319.